



Effect of desert sand on the uniaxial compressive properties of mortar after elevated temperature

Qian Zhang ^a, Qiang Liu ^a, Haifeng Liu ^a  , Jialing Che ^a, Xiaolong Chen ^a, Shu Ing Doh ^b

Show more 



Outline



Share



Cite

<https://doi.org/10.1016/j.pce.2020.102962>

[Get rights and content](#)

Highlights

- Desert sand was used as fine aggregate to prepare mortar.
- The mechanical properties of desert sand mortar after high temperature were studied.
- The compression constitutive model of desert sand mortar after high temperature was established.

Abstract

In China, medium sand is widely used for engineering applications. However, over quarrying of medium sand to meet the demand for urbanization has led to the environmental issue. The arid area of Northwest China, which has high concentration of desert could provide sufficient supply of desert sand for engineering applications. In this paper, desert sand was used to replace medium sand to produce desert sand mortar (DSM). The uniaxial compression test was performed on the DSM undergoing elevated temperature treatment, and the stress-strain

curves of the DSM after different temperatures were obtained. The effects of temperature and desert sand replacement rate (DSR) on the peak stress, peak strain, elastic modulus, Poisson's ratio, and mass loss rate of DSM was analysed. The test results showed that with the increase of DSR, the peak stress and elastic modulus of DSM first increased and then decreased. As the temperature increased, the Poisson's ratio of the DSM decreased first and then increased. Based on regression analysis, the relationships between peak stress, peak strain, elastic modulus, Poisson's ratio of DSM, temperature, and DSR were obtained. At the same time, a one-parameter compression constitutive equation of DSM after the elevated temperature was established. Since the equation has only one parameter, the calculation process was greatly simplified based on ensuring the calculation results. The model was in high agreement with the test results. This equation can provide a reference for further studies in the field of mechanical properties of DSM and desert sand concrete (DSC) after elevated temperatures.

 Previous

Next 

Keywords

Constitutive equation; Desert sand mortar; Elevated temperature; Stress-strain curve; Uniaxial compression

1. Introduction

Article II. Sand is one of the most consumed natural resources which is essential for the preparation of concrete.

Article III. By mixing suitable amount of sand, concrete can achieve the optimal mix ratio with only small amount of cement. About 50 billion tons of fine aggregates are used every year, which is more than enough to blanket the entire UK ([BBC NEWS](#)). However, the high demand of sand due to development has cause scarcity of sand forcing some countries to import sand from other countries. In the current research trend focuses on using industrial byproduct such as copper slag ([Chithra et al., 2016](#); [Vijayaraghavan et al., 2017](#)), blast furnace slag ([Aliabdo et al., 2019](#); [Shen et al., 2019](#)), fly ash ([Tuinukuafe et al., 2019](#); [Singh et al., 2019](#)) to replace sand. China has wide desert area of approximately 1.28 million square kilometers with 80% of the desert are concentrated in the arid zone of northwest China. Therefore, from the perspective of ecology and cost, it is more beneficial to use desert sand to produce concrete. Over the year, many studies have been conducted on desert sand. However, those researches only study on the effect of DSR ([Zhang et al., 2019](#); [Che et al., 2019](#)), water to cement ration ([Yan et al., 2019](#); [Liu et al., 2017a](#)), cement to sand ratio ([Benabed et al., 2014](#)), high strength DSC ([Yang et al., 2014, 2015](#)), dynamic mechanical properties of DSC ([Liu et al., 2017b](#)) and etc. Luo ([Luo et al., 2013](#)) and Al-Harthy ([Al-Harthy et al., 2007](#)) still discussed the effects of dune

sand on the mechanical properties of concrete. Very minimum studies have been conducted on DSC from the perspective of elevated temperature.

At present, building fires have become one of the most common and easily-caused disasters. The statistics of building fires in China, as shown in [Table 1](#).

Table 1. The statistics of building fires in China ([China Fire Yearbook, 2013](#), [China Fire Yearbook, 2014](#), [China Fire Yearbook, 2015](#)).

Years	Occurrences	Deaths	Injuries	Direct loss/million ¥	Burned building/m ²
2013	89005	968	526	174.6625	4180544
2014	202299	1962	1448	376.0282	7048557
2015	197427	1720	1259	353.8072	6985867

Building fire accelerates the concrete deterioration through water-fire coupling effort which reduces the carrying capacity of a structure. In this regard, some researchers ([Ren et al., 2015](#); [Gupta et al., 2017](#)) compared the strength of concrete with natural cooling and water cooling. Due to different cooling methods, the result indicated that the peak stress after natural cooling is better than the water cooling. Liu ([Liu and Liu, 2018](#)) conducted both microscopic analysis on specimens with elevated temperature. The result revealed that the modulus of elasticity of DSC gradually decreases with the increase of temperature, from room temperature (20 °C) to 500 °C. The optimum modulus of elasticity for DSC was at 40% DSR. The same result is confirmed by Sun ([Sun and Liu, 2018](#)) for both flexural strength and splitting tensile. Sun ([Sun and Liu, 2018](#)) found that as the temperature increase, the concrete with higher DSR has lower ultrasonic loss and lower porosity rate.

Concrete is composed of aggregate and mortar. During the loading process, if the elastic modulus and Poisson's ratio of coarse aggregate and mortar are significantly different, it will lead to inconsistent deformation between them. As a result, the concrete structure is damaged, and the bearing capacity is reduced. Therefore, in order to study the mechanical properties of DSC and DSM after elevated temperature, six target temperatures and six substitution rates were set, the maximum temperature was 700 °C. This paper conducted a uniaxial compression test on DSM after elevated temperature, and obtained the stress-strain curve. Through experiments, the peak stress, elastic modulus, peak strain and Poisson's ratio of DSM after elevated temperature were analysed. The relationship between temperature, DSR and peak stress, elastic modulus, peak strain and Poisson's ratio were fitted, respectively. A constitutive equation suitable for this study is obtained. Using desert sand as fine aggregate to prepare DSM and DSC is conducive to reducing project cost, alleviating the pressure of shortage of sand resources, improving urban desertification, and optimizing the ecological environment. Therefore, it is very necessary to study the application of desert sand in practice

2. Materials and method

2.1. Materials and mix ratio

Article IV. The medium sand and desert sand were used to produce DSM. Medium sand was taken from the artificial washing sand from the quarrying industry in Ningxia. Desert sand was taken from Mu Us desert. The physical and mechanical properties of medium sand and desert sand were tabulated in [Table 2](#).

Table 2. Physical and mechanical properties of fine aggregate.

Type of test sand	Corresponding cumulative sieve percentage for different sieve sizes/%						Fineness modulus/%	Bulk density/g·cm ³	Appare Density
	4.75 mm	2.36 mm	1.18 mm	0.6 mm	0.3 mm	0.15 mm			
Medium sand	4.8	32.8	51.2	70.0	85.6	95.3	2.38	1.57	2.64
Desert sand	—	—	0	0.04	2.4	22.3	0.29	1.4	2.62

The chemical components of fine aggregate are shown in [Table 3](#). Comparing with the article ([Che et al., 2019](#)), the desert sand all was derived from Mu Us Desert, however, the content of FeO, CaO, and MgO in desert sand is quite different. It was thought that this difference may be caused by the location and depth of sand extraction. In the test, the cement was 42.5 R ordinary Portland cement. Fly ash was the Class I fly ash, which was produced by a local power plant in Ningxia. The water content was 0.2%, and the burning loss was 2.8%. The superplasticizer was a polycarboxylic acid superplasticizer with high performance. The mix proportion of DSM are shown in [Table 4](#).

Table 3. Chemical components of fine aggregate.

Type of test sand	Component/%							
	SiO ₂	FeO	Al ₂ O ₃	CaO	MgO	Na ₂ O	K ₂ O	Loss on ignition
Medium sand	86.55	0.98	9.74	0.96	1.09	—	—	—
Desert sand	82.66	1.85	8.72	2.00	1.51	0.07	0.12	2.8

Table 4. Mix proportion of DSM.

DSR/%	Fly ash Dosage/%	Mixing ratio per unit volume of concrete/kg.m ⁻³				
		water	cement	fly ash	medium sand	desert sand
0	10	285	570	69	1278	0
20		285	570	69	1023	255
40		285	570	69	767	512
60		285	570	69	512	767
80		285	570	69	255	1023
100		285	570	69	0	1278

2.2. Physical properties of freshly mixed DSM

Article V. The physical properties of various fresh DSM were tested following *the Standard for Test Methods of Basic Performance of Building Mortar (JCJ/T 70–2009)* ([Shanxi Provincial Academy of Building Sciences, 2009](#)). In [Table 5](#), with the increase of DSR, the immersion and stratification of DSM gradually decreased. The apparent density increases from 0 to 40% first, then reduces from 40% to 100%. Since the fineness modulus of desert sand is only 0.292, compared with ordinary mortar (0%), as the replacement rate increases, the water demand is greater. Therefore, in the case of constant water consumption, the degree of immersion decreases. As shown in [Table 5](#), the maximum difference in DSM stratification is 6 mm. Using desert sand instead of medium sand can effectively improve the compactness of DSM. However, when the replacement rate exceeded 40%, the gradation and uniformity of DSM were reduced, resulting in a decrease in the apparent density of DSM.

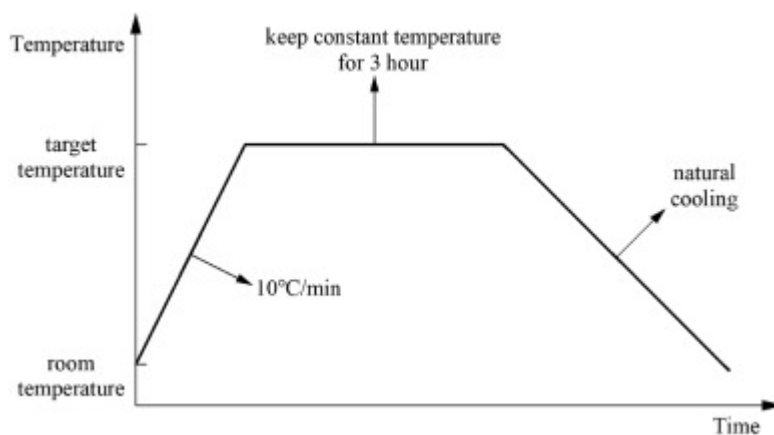
Table 5. Physical properties of DSM.

Indicator name	DSR-0%	DSR-20%	DSR-40%	DSR-60%	DSR-80%	DSR-100%
Immersion/cm	9.9	9.3	8.5	7.8	7.4	7.1
Stratification/cm	1.3	1.1	1.0	0.9	0.8	0.7
Apparent density/kg.m ⁻³	2230	2276	2295	2246	2187	2168

2.3. Elevated temperature test

In this paper, the size of the test specimens were prisms of 40 mm × 40 mm × 160 mm. Considering six DSR and six temperatures, six test specimens were prepared at the same temperature in each DSR, a total 216 test specimens were required. The preparation of the DSM mixture was carried out following *the Standard for Test Methods of Basic Performance of Building Mortar (JC/T 70–2009)* (Shanxi Provincial Academy of Building Sciences, 2009). After the specimens were made for 24 h, the specimens were demolded and placed in a standard curing room for 28 days. Subsequently, the test specimens were oven dried at a constant temperature of 50 °C for 24 h, and then subjected to an elevated temperature test.

When performing elevated temperature tests, there were often differences in the setting of the maximum temperature value. The highest temperature was 600 °C (Pliya et al., 2019), 700 °C (Kim and Gyu-Phil, 2015), and some were more than 700 °C (Qiu, 2019; Kienzler et al., 2014; Fernández et al., 2017). Since the fineness modulus of sand is very small, the use of desert sand instead of medium sand improves the compactness and water retention of DSM. When the temperature was too high, the DSM was prone to burst, which may damage the test equipment. By referring to past literatures (Gupta et al., 2017; Liu and Liu, 2018), the target temperature was 100 °C, 200 °C, 300 °C, 500 °C, 700 °C. The heating equipment was CSL-26-17 elevated temperature furnace, and the heating rate was 10 °C/min. As shown in Fig. 1, after heating to the target temperature, the constant temperature is maintained for 3 h. The DSM samples were then removed from the high-temperature furnace, and the DSM samples were cooled to room temperature by natural cooling. After three days, the mass of the DSM specimens was measured, while the mechanical properties were tested.



[Download : Download high-res image \(160KB\)](#)

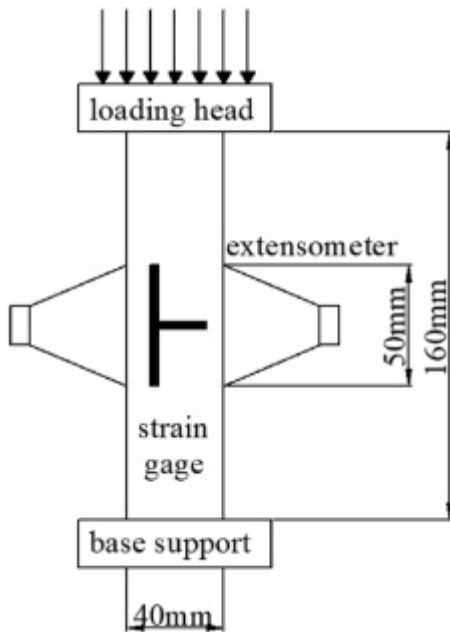
[Download : Download full-size image](#)

Fig. 1. Heating and cooling curve.

2.4. Uniaxial compression test

Article VI. The uniaxial compression test of the prism was carried out by using CMT5305 electronic universal testing machine, and the loading was controlled by displa

loading rate of 0.006 mm/s. The longitudinal and transverse strain gauges were affixed to the front and back sides of the specimen, and the loading diagram was shown in Fig. 2. In order to make the surfaces of the test piece flush, the surfaces of the test piece needed to be polished before heating at the elevated temperature. Before the compressive test started, the test piece needed to be pre-compressed with a compressive strength of about 30%. Three preloads can effectively reduce the error caused by the unevenness of the loading surface and the pressured surface.



[Download : Download high-res image \(169KB\)](#)

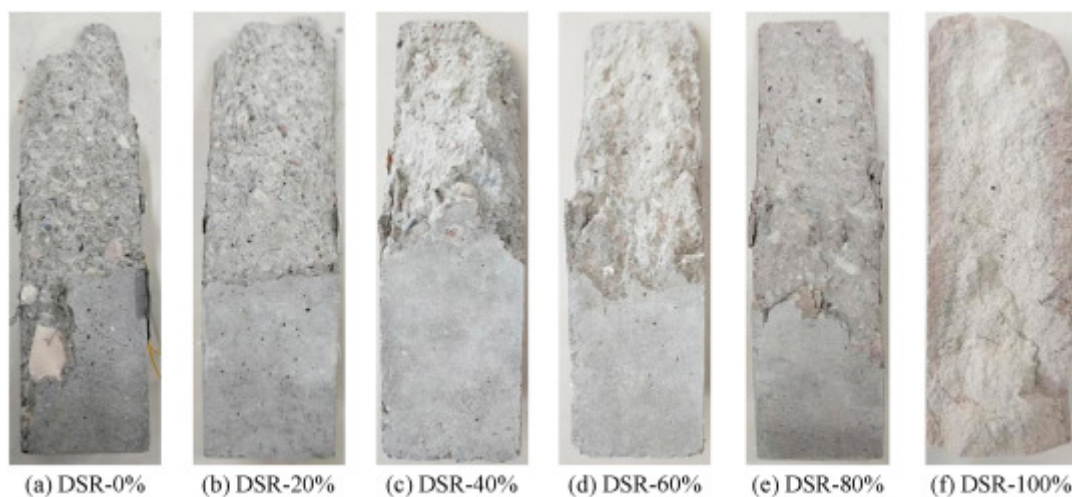
[Download : Download full-size image](#)

Fig. 2. Loading setup.

3. Analysis of test results

3.1. Uniaxial compression failure mode

Article VII. Fig. 3 is a typical photograph of DSM with different DSR after uniaxial compression failure. From Fig. 3, the failure of the DSM was oblique splitting. With the increase of DSR, the oblique splitting failure angle decreased from 0 to 40° first and then increased from 40° to 100°. When the DSR was 100%, the damage was close to horizontal damage. With the increase of the DSR, the denseness of the DSM was improved, and the pore structure was less. Some researchers conducted XRD (Sugiyama and Tsuji, 2008; Tonelli et al., 2017), X-ray (Lerouge et al., 2017) to study the internal changes of concrete. Therefore, in the later tests, similar methods can be used to study the structural damage of the mortar after elevated temperature.



[Download : Download high-res image \(604KB\)](#)

[Download : Download full-size image](#)

Fig. 3. Failure surface of DSM.

3.2. The mass loss rate of DSM after elevated temperature

The mass loss rate of DSM was the ratio of mass change before and after elevated temperature to the mass before elevated temperature. In Fig. 4, the mass loss rate of DSM gradually increased with the increasing temperature. According to the literature (Annerel and Taerwe, 2009; Hager, 2013; Sun and Miao, 2012), when the temperature was lower than 300 °C, a large amount of free and combined water evaporated inside the specimen, and the mass loss rate increased significantly. At 300 °C–500 °C, the free water and bound water inside the mortar specimens were basically evaporated, part of the hydrated calcium silicate (C–S–H) was dehydrated, and a small amount of $\text{Ca}(\text{OH})_2$ was decomposed, so that the mass loss rate continued to increase. After the temperature exceeded 500 °C, the $\text{Ca}(\text{OH})_2$ in the mortar sample was decomposed, and a large amount of calcium silicate hydrate (C–S–H) was dehydrated. The mass loss rate after 500 °C was significantly improved compared with the mass loss rate of 300 °C–500 °C.

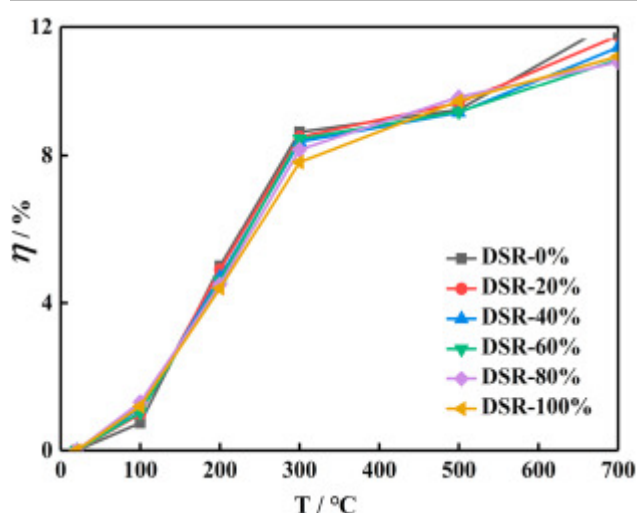



Fig. 4. Relationship between mass loss rate and temperature.

3.3. Test results of uniaxial compression mechanical properties of DSM

Article VIII. [Table 6](#) shows the test results of uniaxial compression of DSM after elevated temperature. The peak strain in the table was the corresponding strain value at the peak stress, which was obtained from the test. The elastic modulus was taken as the secant modulus at 40% peak stress, and the Poisson's ratio was the ratio of transverse strain to longitudinal strain in the elastic stage of the stress-strain curve.

Table 6. Test results of DSM under uniaxial compression after elevated temperature.

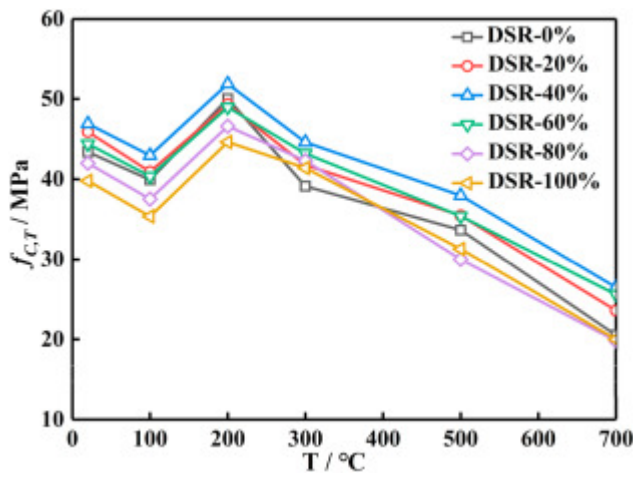
Parameter	T/°C	Test results of different DSR					
		0% 0%	20%	40%	60%	80%	100%
Peak stress/MPa	room temperature	43.41	45.92	46.91	44.41	42.11	39.84
	100	39.93	40.93	42.97	40.37	37.53	35.37
	200	50.03	49.33	51.87	48.97	46.57	44.63
	300	39.14	41.77	44.60	43.22	42.32	41.38
	500	33.67	35.67	37.97	35.41	30.03	31.33
	700	20.53	23.65	26.49	25.63	19.82	20.01
Peak strain/ 10^{-3}	room temperature	3.01	2.84	2.92	2.72	2.59	2.57
	100	2.81	2.79	2.83	2.71	2.54	2.48
	200	2.87	2.83	2.83	2.76	2.67	2.47
	300	3.67	3.58	3.52	3.36	3.34	3.34
	500	5.25	5.09	4.96	4.57	4.47	4.50
	700	6.47	6.11	5.72	5.86	5.85	5.65
Elastic Modulus/GPa	room temperature	26.03	27.74	27.96	27.49	26.33	25.84
	100	22.06	23.42	23.69	22.81	21.12	20.5
	200	24.87	25.7	26.16	25.54	23.64	23.07
	300	14.01	14.66	16.10	15.23	FEEDBACK 	

Parameter	T/°C	Test results of different DSR					
		0% 0%	20%	40%	60%	80%	100%
Poisson's ratio	500	8.12	8.15	8.71	8.58	7.90	8.12
	700	3.25	4.65	5.52	4.87	4.15	4.17
	room temperature	0.215	0.210	0.198	0.192	0.185	0.181
	100	0.191	0.184	0.182	0.180	0.174	0.172
	200	0.183	0.176	0.173	0.171	0.165	0.160
	300	0.163	0.158	0.152	0.146	0.142	0.136
	500	0.099	0.103	0.108	0.103	0.094	0.098
	700	0.176	0.175	0.169	0.161	0.145	0.152

3.4. Peak stress of DSM after elevated temperature

3.4.1. Effect of temperature on the peak stress

Article IX. [Fig. 5](#) shows the relationship between the peak stress of DSM and temperature after elevated temperature. According to [Fig. 5](#), at 100 °C, the peak stress of DSM was lower than that at room temperature. When the temperature increased to 200 °C, the peak stress was raised. When the temperature was higher than 200 °C, the peak stresses of DSM decreased with the rise of temperature. This was because when the temperature reaches 100 °C, a small amount of C₂SH(A) was generated in the mortar ([Khoury, 1992](#)). This material has a low specific surface area and has porosity and crystallinity, which accordingly reduced the adhesive force between the slurry ([Khoury, 1992](#)). As a result, the peak stress was reduced. At 200 °C, the cohesion between the gel particles in the DSM sample increased due to a large amount of free water discharged, and the dehydration and hardening of the cement gel increase the peak stress. As the temperature continued to rise, the cement slurry tended to shrink, and the fine aggregate continues to expand ([Annerel and Taerwe, 2009](#); [Cruz and Gillen, 1980](#)). There was a massive thermal strain difference between the fine aggregate and the cement slurry, which weakened the adhesion between them and causes cracks. Meanwhile, in the range of 500 °C–650 °C, α-type quartz becomes β-type quartz, and its volume increases ([Khoury, 1992](#); [Dong, 2001](#)), which exacerbated the destruction of the internal structure of the mortar, and made the peak stress of the mortar sharply decrease.

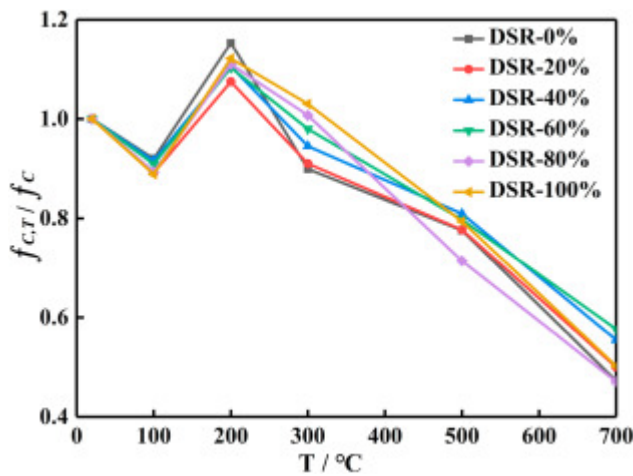


[Download : Download high-res image \(291KB\)](#)

[Download : Download full-size image](#)

Fig. 5. Relationship between the peak stress of DSM and temperature.

Fig. 6 shows the relationship between the relative peak stress of DSM and temperature. It observed from Fig. 6 that at the range of 100 °C–200 °C, the strength of the DSM about 90% and 110% of the peak stress at room temperature, respectively. The relative peak stress of DSM decreased with the increase of temperature.



[Download : Download high-res image \(294KB\)](#)

[Download : Download full-size image](#)

Fig. 6. Relationship between relative peak stress of DSM and temperature.

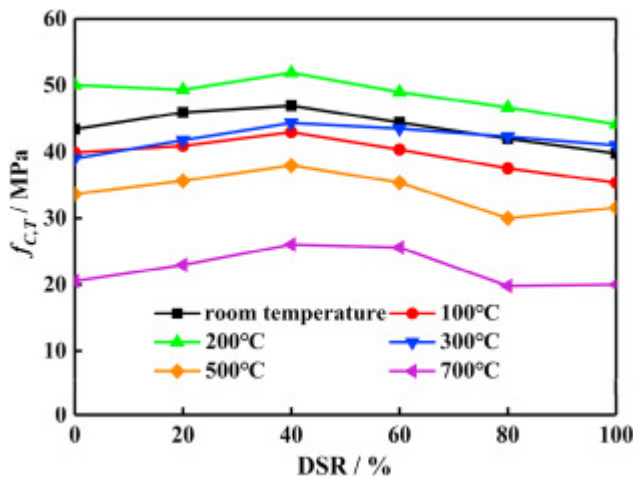
Based on the literature (Popovics, 1973), the fitting relationship between the peak stress of DSM, temperature, and DSR was established, as shown in the following formula:

$$\frac{f_c(S,T)}{f_c} = \begin{cases} 1.016 - 1.84 \left(\frac{T-20}{700} \right) + 0.23S + 8.99 \left(\frac{T-20}{700} \right)^2 - 0.075S \left(\frac{T-20}{700} \right) - 0.338S^3, 20 \\ {}^\circ C \leq T \leq 200^\circ C \\ 1.282 - 0.74 \left(\frac{T-20}{700} \right) + 0.3S - 0.062 \left(\frac{T-20}{700} \right)^2 + 0.011S \left(\frac{T-20}{700} \right) - 0.365S^3, 200 \\ {}^\circ C \leq T \leq 700^\circ C \end{cases} \quad (1)$$

where $f_c(S, T)$ is the peak stress of DSM after elevated temperature, **MPa**. f_c is the peak stress of ordinary mortar at room temperature, **MPa**. T is temperature, $^\circ C$. S is DSR, %. The coefficient of determination (R^2) of this formula is 0.97, and the fitting degree is good.

3.4.2. Effect of DSR on peak stress

Article X. Fig. 7 reveals the relationship between the peak stress of DSM and the replacement rate of desert sand after elevated temperature. From Fig. 7, the peak stress of the DSM was increased first and then decreased with the rise of the DSR after elevated temperature. The peak stress of the DSM reached the maximum at 40% of the DSR at different temperatures. The fineness modulus of the desert sand was only 0.292. After adding desert sand to the mortar, the gradation of the aggregate was improved, and the internal structure was more uniform and denser, so the strength of the DSM was improved. However, desert sand was the product of long-term weathering of loose parent rock, and its strength was lower than the medium sand. For the DSM, when the DSR exceeded the optimal replacement rate, the strength of the DSM was gradually decreased.



[Download : Download high-res image \(278KB\)](#)

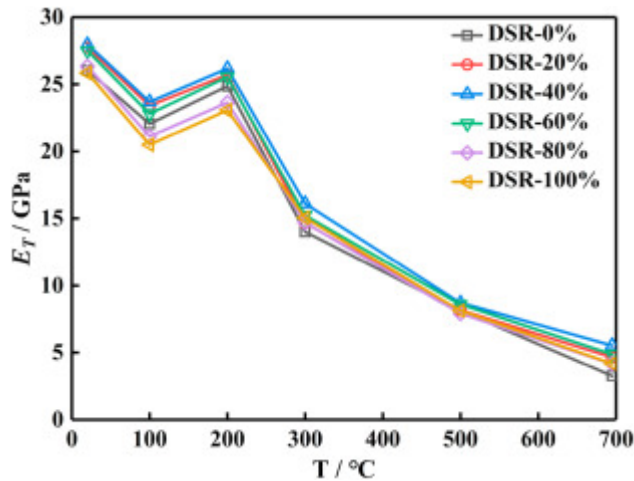
[Download : Download full-size image](#)

Fig. 7. Relationship between DSR and peak stress.

3.5. Elastic modulus of DSM after elevated temperature

3.5.1. Effect of temperature on the elastic modulus

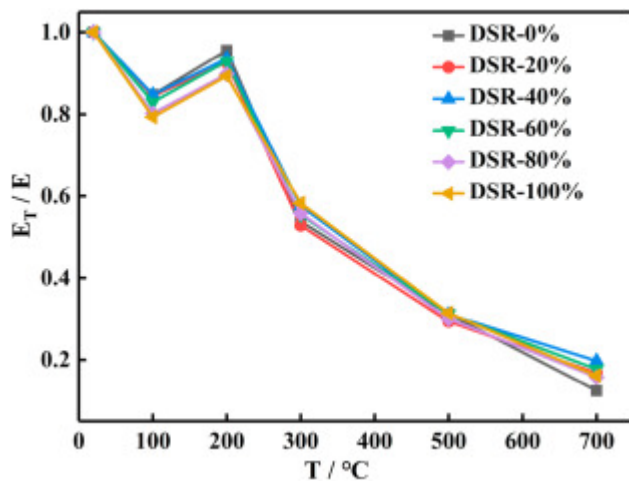
Article XI. After elevated temperature, the relationship between the elastic modulus of DSM and temperature can be seen from Fig. 8, and the relationship between the relative elastic modulus of DSM and temperature can be seen from Fig. 9. From Figs. 8 and 9, at 100 °C, the elastic modulus of the DSM was lower than that at room temperature, which was 80%–90% of the elastic modulus at room temperature. The elastic modulus reached 90%–95% of the elastic modulus at room temperature. The elastic modulus decreased sharply at 200 °C–300 °C. When the temperature exceeded 300 °C, the decrease in elastic modulus was slowed down. At 700 °C, the elastic modulus was 10%–20% of the elastic modulus at room temperature.



[Download : Download high-res image \(269KB\)](#)

[Download : Download full-size image](#)

Fig. 8. Relationship between elastic modulus of DSM and temperature.



[Download : Download high-res image \(248KB\)](#)

[Download : Download full-size image](#)

Fig. 9. Relationship between relative elastic modulus of DSM and temperature.

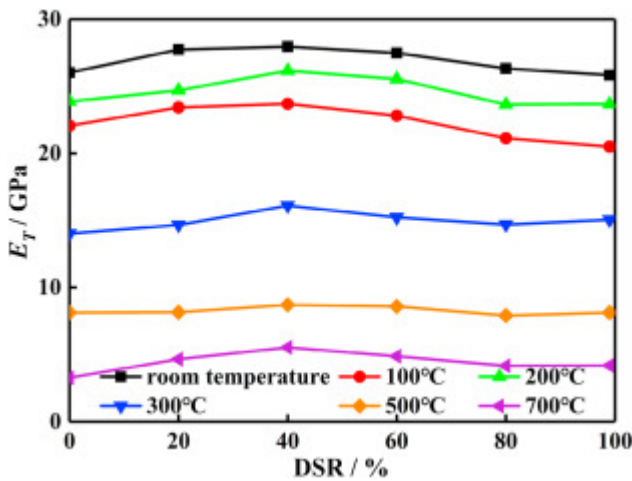
The formula of the elastic modulus of DSM, temperature and the DSR after the elevated temperature was fitted, as follows:

$$\frac{E(S,T)}{E} = \begin{cases} 1.02 - 2.45 \left(\frac{T-20}{700} \right) + 0.25S + 8.74 \left(\frac{T-20}{700} \right)^2 - 0.21S \left(\frac{T-20}{700} \right) - 0.24S^3, & 20^\circ\text{C} \leq T \leq 700^\circ\text{C} \\ 1.61 - 3.11 \left(\frac{T-20}{700} \right) + 0.12S + 1.66 \left(\frac{T-20}{700} \right)^2 + 0.09S \left(\frac{T-20}{700} \right) - 0.19S^3, & 20^\circ\text{C} \leq T \leq 700^\circ\text{C} \end{cases} \quad (2)$$

where $E(S, T)$ is the elastic modulus of DSM after elevated temperature, **GPa**. E is the elastic modulus of ordinary mortar at room temperature, **GPa**. The coefficient of determination (R^2) of this formula is greater than 0.967, and the fitting degree is good.

3.5.2. Impact of DSR on elastic modulus

Article XII. Fig. 10 reveals the relationship between the elastic modulus of DSM and the replacement rate of desert sand after elevated temperature. From Fig. 10, the elastic modulus of the DSM increased first and then decreased with the increase of the replacement rate of the desert sand after elevated temperature. The elastic modulus of the DSM reached the maximum when the DSR was 40%.



[Download : Download high-res image \(252KB\)](#)

[Download : Download full-size image](#)

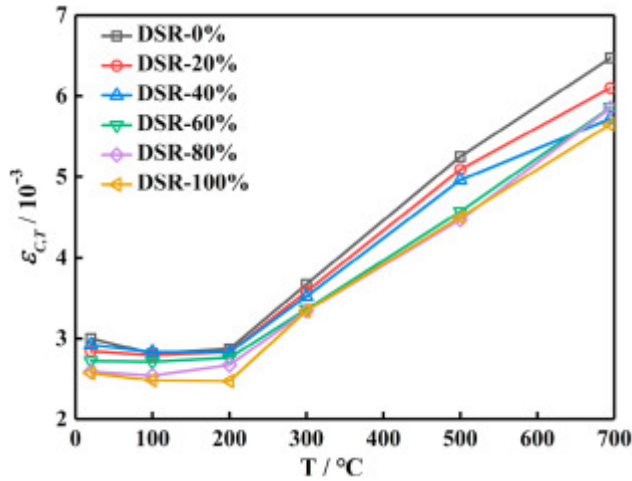
Fig. 10. Relationship between DSR and elastic modulus.

3.6. Peak strain of DSM after elevated temperature

3.6.1. Effect of temperature on peak strain

Article XIII. After elevated temperature, the relationship between the peak strain and temperature of DSM under uniaxial compression can be seen in Fig. 11, and the relationship between the relative peak strain and temperature of DSM can be seen in Fig. 12. In Figs. 11 and 12, when the temperature was lower than 200 °C, the peak strain of DSM

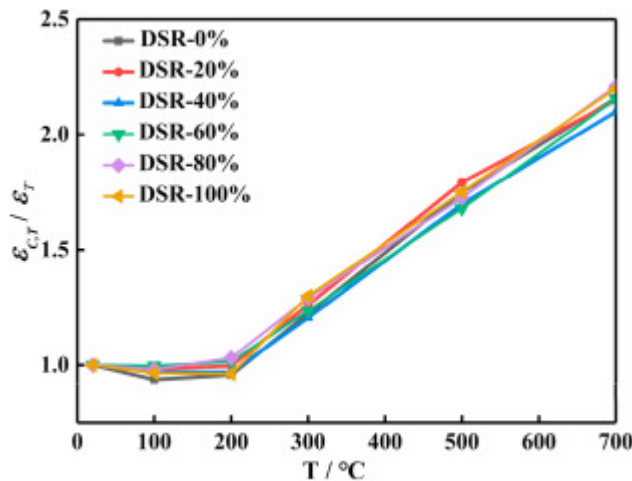
much. When the temperature was higher than 200 °C, the peak strain of DSM showed a linear increasing trend. This is because when the temperature was less than 200 °C, the fine aggregate and the slurry polymer are in a slightly expanded state, and the expansion rate was similar. The compactness inside the DSM was equivalent to that at room temperature, and the peak strain was basically unchanged. When the temperature exceeded 200 °C, the fine aggregate continued to expand. At the same time, the slurry polymer volume shrunk sharply, which caused the mortar interior to become porous and loose (Yang et al., 2015), and the peak strain increased significantly.



[Download : Download high-res image \(288KB\)](#)

[Download : Download full-size image](#)

Fig. 11. Relationship between the peak strain of DSM and temperature.



[Download : Download high-res image \(254KB\)](#)

[Download : Download full-size image](#)

Fig. 12. Relationship between the relative peak strain of DSM and temperature.

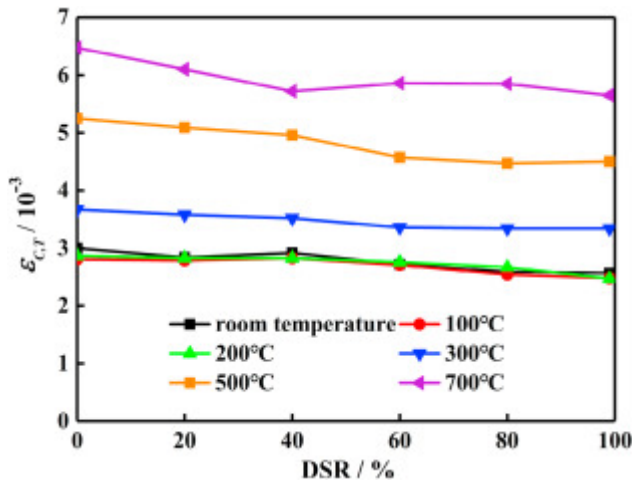
The relationship between the peak strain of DSM, temperature and the replacement rate of desert sand after the elevated temperature was fitted, as follows,

$$\frac{\epsilon_c(S,T)}{\epsilon_c} = 0.93 + 0.42 \left(\frac{T-20}{700} \right) - 0.155S + 0.863 \left(\frac{T-20}{700} \right)^2 - 0.14S \left(\frac{T-20}{700} \right) + 0.042S^2 \quad (3)$$

where $\epsilon_c(S,T)$ is the peak strain of DSM after elevated temperature, $\times 10^{-3}$. ϵ_c is the peak strain of ordinary mortar at room temperature, $\times 10^{-3}$. The coefficient of determination (R^2) of this formula is 0.972, and the fitting degree is good.

3.6.2. Effect of DSR on peak strain

Article XIV. Fig. 13 reveals that the relationship between the peak strain of DSM and the replacement rate of desert sand after elevated temperature. It can be known from Fig. 13 that the peak strain of the DSM gradually decreased with the increase of the DSR after elevated temperature.



[Download : Download high-res image \(243KB\)](#)

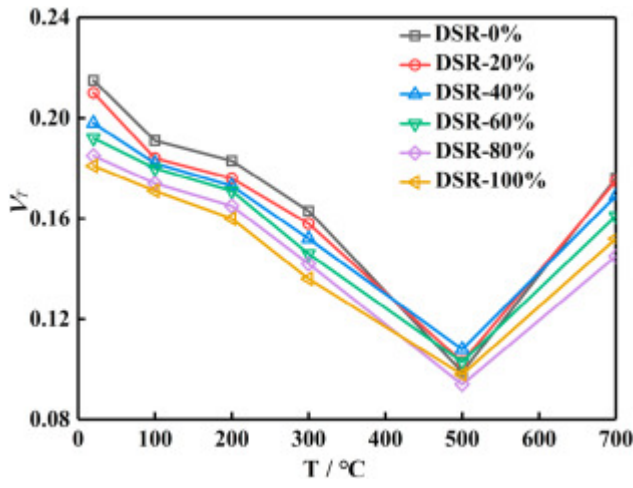
[Download : Download full-size image](#)

Fig. 13. Relationship between DSR and peak strain.

3.7. Poisson's ratio of DSM after elevated temperature

3.7.1. Influence of temperature on Poisson's ratio

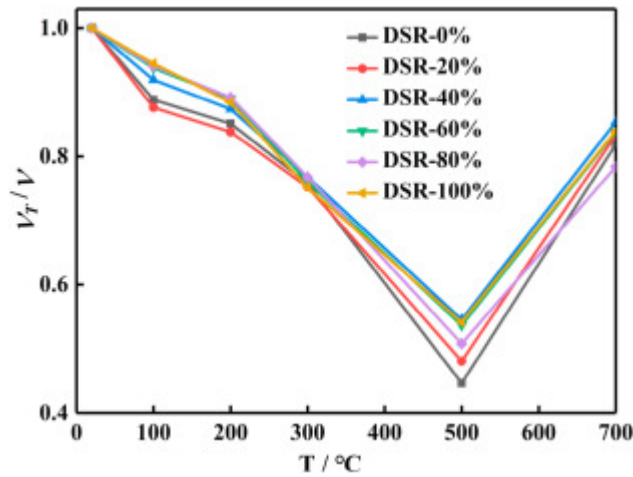
Article XV. The relationship between Poisson's ratio of DSM and temperature are shown in Fig. 14. The relationship between the relative Poisson's ratio of DSM and temperature can be found in Fig. 15. By referring to Figs. 14 and 15, when the temperature was lower than 500 °C, the Poisson's ratio decreased with increasing temperature. After 500 °C, the Poisson's ratio of DSM dropped to a minimum, which was 45%–55% of Poisson's ratio at room temperature. After 500 °C, the Poisson's ratio gradually increases as the temperature continues to increase. After 700 °C, Poisson's ratio of DSM reaches about 80% at room temperature.



[Download : Download high-res image \(297KB\)](#)

[Download : Download full-size image](#)

Fig. 14. Relationship between Poisson's ratio of DSM and temperature.



[Download : Download high-res image \(275KB\)](#)

[Download : Download full-size image](#)

Fig. 15. Relationship between relative Poisson's ratio of DSM and temperature.

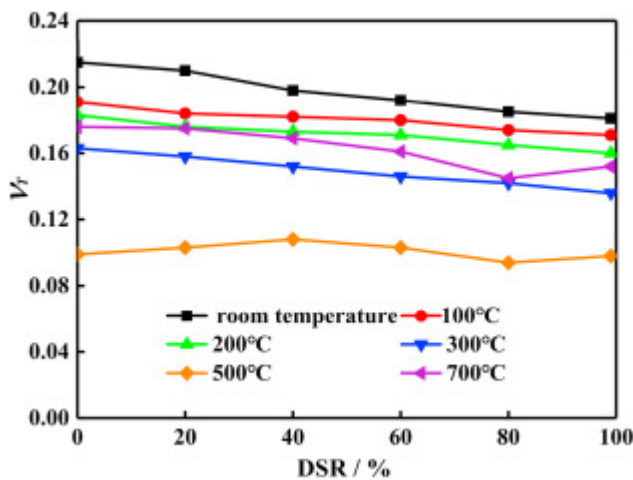
The relationship between Poisson's ratio of DSM, temperature and DSR after elevated temperature was fitted as follows:

$$\frac{\nu(S,T)}{\nu} = 0.972 + 0.056 \left(\frac{T-20}{700} \right) - 0.157S - 2.971 \left(\frac{T-20}{700} \right)^2 + 0.336 \times S \times \left(\frac{T-20}{700} \right) + 2.83 \left(\frac{T-20}{700} \right)^3 - 0.315S \left(\frac{T-20}{700} \right)^2 \quad (4)$$

where $\nu(S, T)$ is Poisson's ratio of DSM after the elevated temperature; ν is Poisson's ratio of ordinary mortar at room temperature. The coefficient of determination (R^2) of this formula is 0.976, and the fitting degree is good.

3.7.2. Impact of DSR on Poisson's ratio

Fig. 16 shows the relationship between Poisson's ratio of DSM and DSR after elevated temperature. From Fig. 16, the Poisson's ratio of DSM decreased gradually with the increase DSR after elevated temperature.



[Download : Download high-res image \(281KB\)](#)

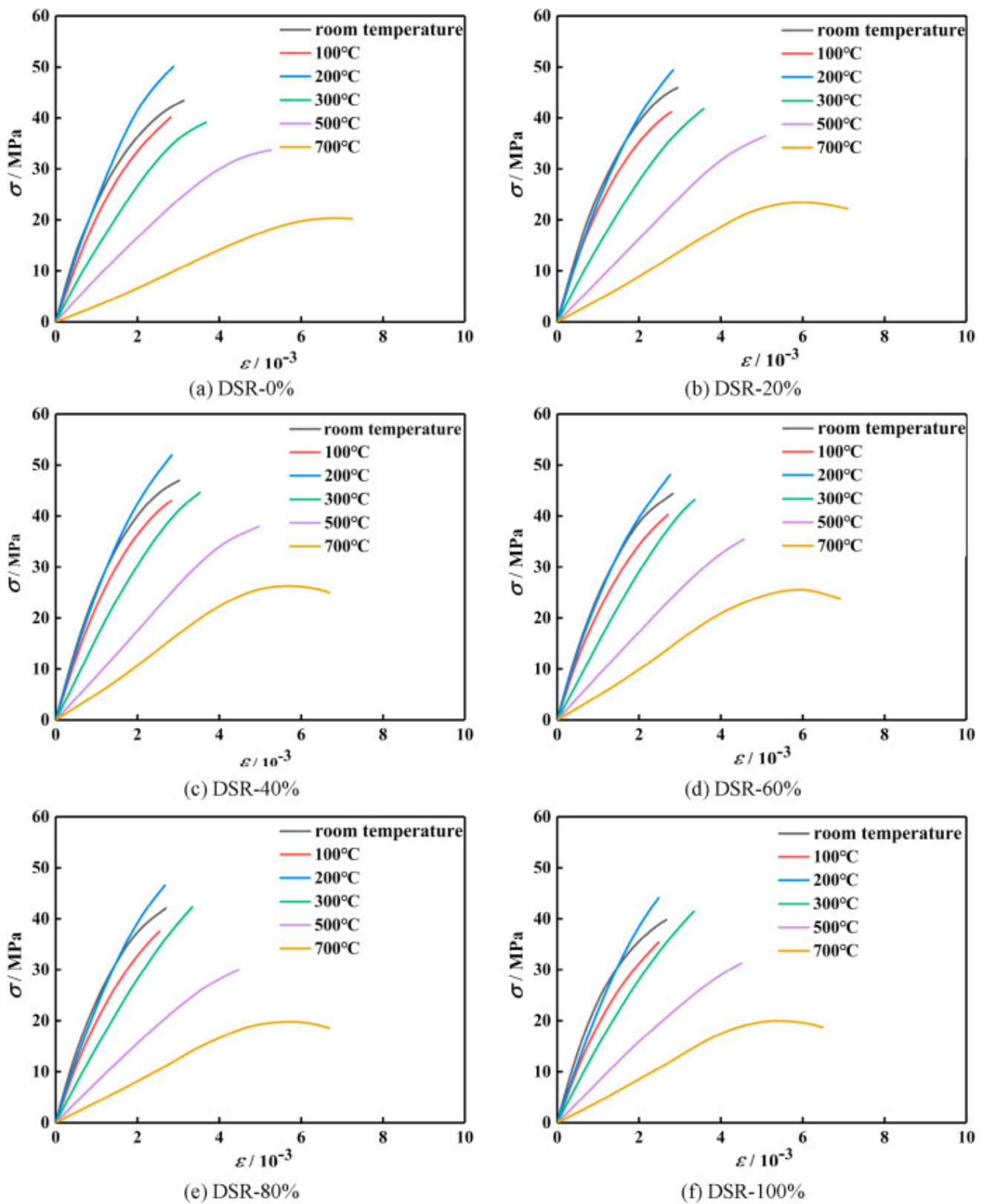
[Download : Download full-size image](#)

Fig. 16. Relationship between DSR and Poisson's ratio of DSM.

4. Stress-strain curve of DSM after elevated temperature

4.1. Stress-strain curve of DSM after different temperatures

The uniaxial compressive stress-strain curve of DSM after the elevated temperature is shown in Fig. 17. From Fig. 17, the uniaxial compression stress-strain curves of DSM were very similar after different temperatures. When the temperature was lower than 500 °C, there was no obvious softening stage of the stress-strain curve of DSM, and the damage was relatively sudden. When the temperature was higher than 700 °C, the stress-strain curve has the visible softening stage.



[Download : Download high-res image \(1MB\)](#)

[Download : Download full-size image](#)

Fig. 17. Stress-strain curve of DSM after elevated temperature.

4.2. Stress-strain curves of DSM at different DSRs

Fig. 18 shows the uniaxial compressive stress-strain curve of DSM under different DSR. It can be seen from Fig. 18 that with the increase of the DSR, the plastic deformation of the DSM under uniaxial compression gradually decreased, which indicated that the deformation modulus gradually decreases. When the DSM was brittle, the destruction of it was more sudden. Under different DSR, the stress-strain curves of DSM were roughly the same with temperature changes, and the curve shows a trend which is steep in the beginning and plateau at the ends.

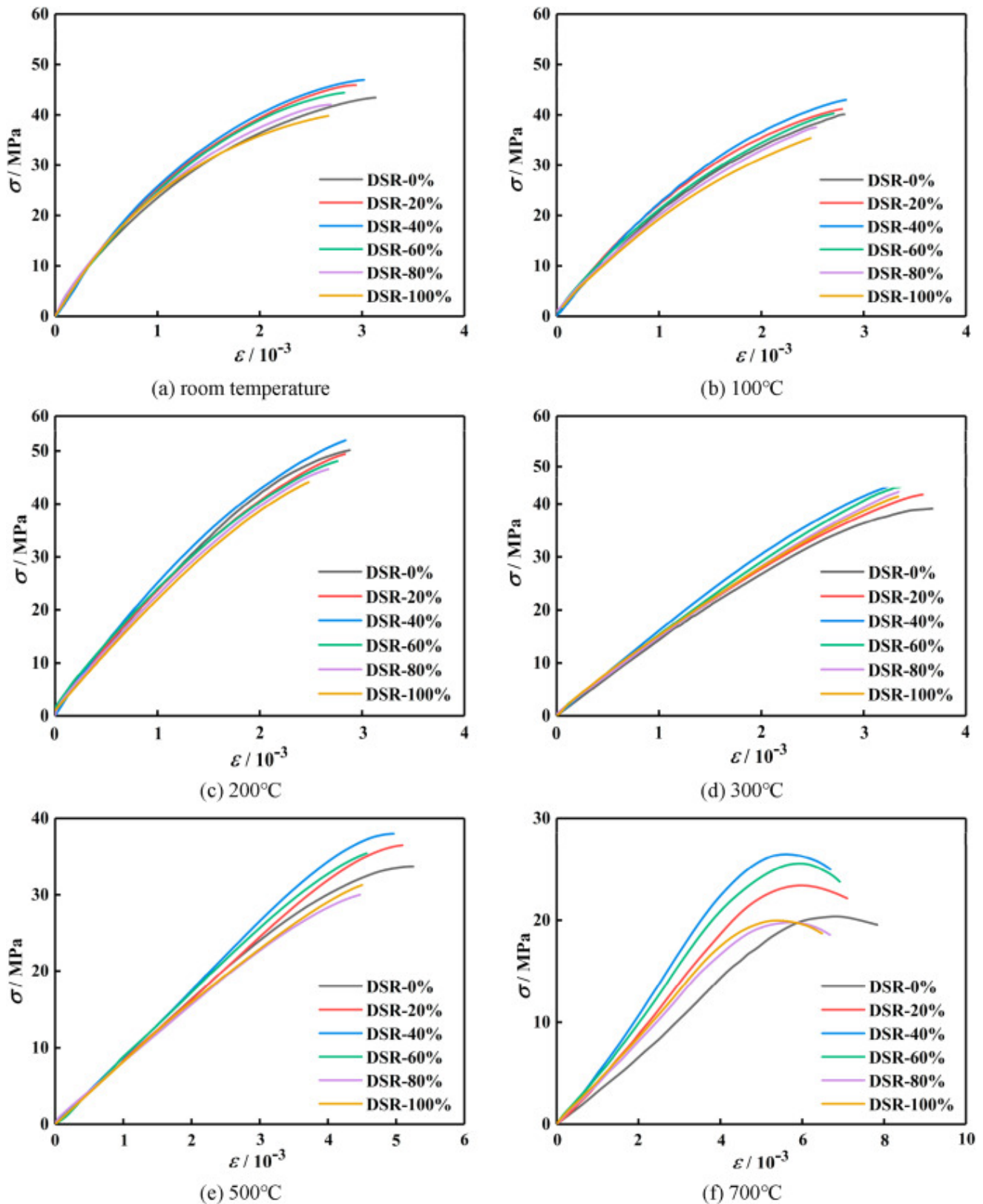


Fig. 18. Stress-strain curve of DSM with different DSR.

4.3. Stress-strain constitutive equation under uniaxial compression

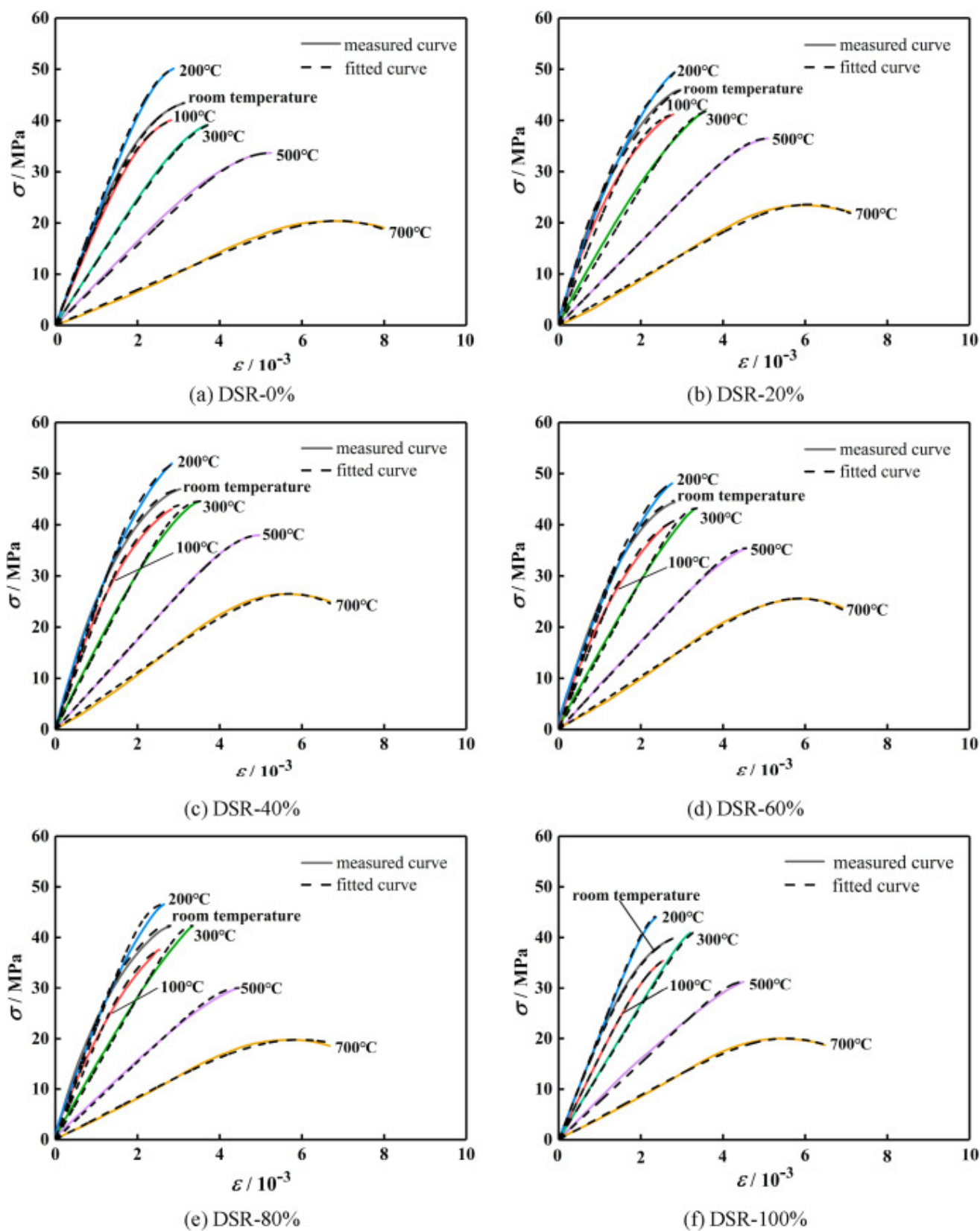
There were many constitutive equations on the stress-strain relationship of concrete under elevated temperatures at home and abroad. In this paper, the constitutive equation (Popovics, 1973) established by Sandor Popovics is selected, which is relatively simple and can be used for mortar and concrete. The parameter n in the constitutive equation can be obtained by fitting. The expression was as follows:

$$\frac{\sigma}{\sigma_c} = \frac{\varepsilon n}{\varepsilon_c} \left(n - 1 + \left(\frac{\varepsilon}{\varepsilon_c} \right)^{-n} \right) \quad (5)$$

where σ and ε are stress and strain respectively, σ_c and ε_c are peak stress and peak strain, respectively, n is a function of temperature (T) and DSR (S), obtained by fitting:

$$\begin{aligned} n = & 2.56 - 2.53 \left(\frac{T-20}{700} \right) - 0.1S + 38.91 \left(\frac{T-20}{700} \right)^2 + 8.07S \left(\frac{T-20}{700} \right) - 60.86 \left(\frac{T-20}{700} \right)^3 \\ & + 25.67S \left(\frac{T-20}{700} \right)^2 + 27.24 \left(\frac{T-20}{700} \right)^4 - 34.28S \left(\frac{T-20}{700} \right)^3 \end{aligned} \quad (6)$$

Comparing the stress-strain curve obtained by formula (5) with the stress-strain curve obtained by the experiment, as shown in Fig. 19, it was found that the two curves agree well.



[Download : Download high-res image \(1MB\)](#)

[Download : Download full-size image](#)

Fig. 19. Comparison of test and calculated stress-strain curve.

5. Conclusion

In this paper, five temperature levels were considered. After elevated temperature, the compressive strength of DSM was tested, and the effects of elevated temperature and DSR on the peak stress, elastic modulus, peak strain and Poisson's ratio of DSM were analysed. This study can provide a reference for the damage assessment of DSC structures after a fire. The main conclusions are as follows:

As the replacement rate of the desert sand increases, the peak stress and elastic modulus of DSM increased first and then decreased. When the DSR was 40%, the peak stress and elastic modulus of DSM reached the maximum value. With the increase of DSR, the peak strain and Poisson's ratio of the specimens decreased slightly.

With the rise of temperature, Poisson's ratio of the DSM decreases first and then increases. At 500 °C, Poisson's ratio of DSM reached the minimum value. When the temperature was lower than 200 °C, the peak strain of DSM not changed much. When the temperature was higher than 200 °C, the peak strain of DSM increased linearly.

With the increase of temperature, the peak stress and elastic modulus of DSM had the same trend. At 100 °C, the peak stress and elastic modulus of DSM decreased. When the temperature increased to 200 °C, the peak stress and elastic modulus of DSM increased. After 200 °C, with the increase of temperature, the peak stress and elastic modulus of DSM gradually decreased.

Considering the effects of temperature and DSR, a single parameter compression constitutive model of DSM after the elevated temperature was established. This equation can provide a reference for further studies in the field of mechanical properties of DSM and DSC after elevated temperatures.

DSR has a greater impact on DSM. Compared with the influence of DSR, the influence of temperature on mortar is more significant, which can provide reference for the application of desert sand as fine aggregate in engineering.

Availability of data and materials

The data and materials had been included in the manuscript.

Author contribution

Qian Zhang and Qiang Liu performed the experiments. Haifeng Liu provided guiding and designed the experiments. Jialing Che and Xiaolong Chen wrote the paper. Shu Ing Doh put forward opinions on writing paper.

Declaration of competing interest

The authors declare that they have no known competing financial interests or personal relationships that could have appeared to influence the work reported in this paper.

Acknowledgments

Article XVI. The project is supported by Science Foundation of Ningxia (2020AAC03044 and 2020AAC03041); National Natural Science Foundation of China (No.11162015 and 51408328), Scientific and technological research project of institutions of higher learning in Ningxia (NGY 2018-1) and Innovation team project of Yangtze River scholars and innovation team development plan (Irt 1067).

[Recommended articles](#)

[Citing articles \(0\)](#)

References

[Al-Harthy et al., 2007](#) A.S. Al-Harthy, M. Abdel Halim, R. Taha, K.S. Al-Jabri

The properties of concrete made with fine dune sand

Construct. Build. Mater., 21 (8) (2007), pp. 1803-1808

[Article](#)  [Download PDF](#) [View Record in Scopus](#) [Google Scholar](#)

[Aliabdo et al., 2019](#) Ali A. Aliabdo, M. Abd Elmoaty, Elmoaty Abd, Mohammed A. Emam

Factors affecting the mechanical properties of alkali activated ground granulated blast furnace slag concrete

Construct. Build. Mater., 197 (2019), pp. 339-355

[Article](#)  [Download PDF](#) [View Record in Scopus](#) [Google Scholar](#)

[Annerel and Taerwe, 2009](#) Emmanuel Annerel, Luc Taerwe

Revealing the temperature history in concrete after fire exposure by microscopic analysis

Cement Concr. Res., 39 (12) (2009), pp. 1239-1249

[Article](#)  [Download PDF](#) [View Record in Scopus](#) [Google Scholar](#)

[Zhang et al., 2019](#) Minghu Zhang, Haifeng Liu, Shuai Sun, Xiaolong Chen, Shu Ing Doh

Dynamic mechanical behaviors of desert sand concrete (DSC) after different temperatures

Appl. Sci., 9 (19) (2019), p. 4151

[CrossRef](#) [View Record in Scopus](#) [Google Scholar](#)

[BBC NEWS](#) BBC NEWS. " Why the World Is Running Out of Sand." ([EB/OL]).

[Google Scholar](#)

[Benabed et al., 2014](#) Benchaa Benabed, A. Lakhdar, K. El-Hadj, K. Said, A.S.E. Belaidi

Effect of fine aggregate replacement with desert dune sand on fresh properties and strength of self-compacting mortars

J. Adhes. Sci. Technol., 28 (21) (2014), pp. 2182-2195

[CrossRef](#) [View Record in Scopus](#) [Google Scholar](#)

[Che et al., 2019](#) Jialing Che, Dan Wang, Haifeng Liu, Yixin Zhang

Mechanical properties of desert sand-based fiber reinforced concrete (DS-FRC) under uniaxial tension/compression test

Appl. Sci., 5 (2019), pp. 3-4

[View Record in Scopus](#) [Google Scholar](#)

[China Fire Yearbook, 2013](#) China Fire Yearbook

Fire Bureau of the Ministry of Public Security [M]

2013/

China Personnel Press, Beijing (2013)

[Google Scholar](#)

[China Fire Yearbook, 2014](#) China Fire Yearbook

Fire Bureau of the Ministry of Public Security [M]

2014/

Yunnan People's Publishing House, Kunming (2014)

[Google Scholar](#)

[China Fire Yearbook, 2015](#) China Fire Yearbook

Fire Bureau of the Ministry of Public Security [M]

2015/

Yunnan People's Publishing House, Kunming (2015)

[Google Scholar](#)

[Chithra et al., 2016](#) Sankar Chithra, S.R.R. Senthil Kumar, K. Chinnaraju

The effect of Colloidal Nano-silica on workability, mechanical and durability properties of High Performance Concrete with Copper slag as partial fine aggregate

Construct. Build. Mater., 113 (2016), pp. 794-804

[Article](#)  [Download PDF](#) [View Record in Scopus](#) [Google Scholar](#)

[Cruz and Gillen, 1980](#) Carlos R. Cruz, M. Gillen

Thermal expansion of Portland cement paste, mortar and concrete at high temperatures

Fire Mater., 4 (2) (1980), pp. 66-70

[CrossRef](#) [View Record in Scopus](#) [Google Scholar](#)

[Dong, 2001](#) Yuli Dong

Fire Safety Design of Concrete Structures [M]


Science Press, Beijing (2001)

[Google Scholar](#)

[Fernández et al., 2017](#) Raúl Fernández, E. Torresb, Ana I. Ruiza, J. Cuevasa, M.C. Alonsoc, J.L.G. Calvoc, E. Rodríguezd, M.J. Turrero, *et al.*


Interaction processes at the concrete-bentonite interface after 13 years of FEBEX-Plug operation. Part II: bentonite contact


Phys. Chem. Earth, Parts A/B/C, 99 (2017), pp. 49-63


[Gupta et al., 2017](#) Trilok Gupta, S. Siddique, R.K. Sharma, S. Chaudhary
Effect of elevated temperature and cooling regimes on mechanical and durability properties of concrete containing waste rubber fiber
Construct. Build. Mater., 137 (2017), pp. 35-45
[Article](#)  [Download PDF](#) [View Record in Scopus](#) [Google Scholar](#)

[Hager, 2013](#) Izabela Hager
Behaviour of cement concrete at high temperature
Bull. Pol. Acad. Sci. Tech. Sci., 61 (1) (2013), pp. 145-154
[CrossRef](#) [View Record in Scopus](#) [Google Scholar](#)

[Khoury, 1992](#) G.A. Khoury
Compressive strength of concrete at high temperatures: a reassessment
Mag. Concr. Res., 44 (161) (1992), pp. 291-309
[CrossRef](#) [View Record in Scopus](#) [Google Scholar](#)




[Kienzler et al., 2014](#) B. Kienzler, C. Borkela, N. Fincka, S. Hecka, S. Hilppa, M. Schliekera, V. Metza, M. Plaschkea, E. Soballaa, T. Cronb, A. Miassoedov
Characterization and radionuclide retention properties of heat-treated concrete
Phys. Chem. Earth, Parts A/B/C, 70 (2014), pp. 45-52
[Article](#)  [Download PDF](#) [View Record in Scopus](#) [Google Scholar](#)

[Kim and Gyu-Phil, 2015](#) Jihwan Kim, Lee Gyu-Phil
Evaluation of mechanical properties of steel-fibre-reinforced concrete exposed to high temperatures by double-punch test
Construct. Build. Mater., 79 (2015), pp. 182-191
[Article](#)  [Download PDF](#) [View Record in Scopus](#) [Google Scholar](#)

[Lerouge et al., 2017](#) Catherine Lerouge, S. Gaboreaua, S. Grangeona, F. Clareta, F. Warmontb, A. Jennic, V. Cloetd, U. Mader
In situ interactions between opalinus clay and low alkali concrete
Phys. Chem. Earth, Parts A/B/C, 99 (2017), pp. 3-21
[Article](#)  [Download PDF](#) [View Record in Scopus](#) [Google Scholar](#)

[Liu and Liu, 2018](#) Haifeng Liu, Ning Liu
Influence of high temperature on the Axis compressive strength and elastic modulus of desert sand concrete
Bulletin of the chinese ceramic society, 37 (11) (2018), pp. 166-173
[Article](#)  [Download PDF](#) [View Record in Scopus](#) [Google Scholar](#)

[Liu et al., 2017a](#) Haifeng Liu, Hejiao Ma, Ning Liu
Influence of fly ash and desert sand on the carbonation resistance property of concrete
Bulletin of the chinese ceramic society, 11 (2017), pp. 248-253+272
[CrossRef](#) [View Record in Scopus](#) [Google Scholar](#)

- [Liu et al., 2017b](#) Haifeng Liu, Jurong Ma, Yiyang Wang, Jianguo Ning
Influence of desert sand on the mechanical properties of concrete subjected to impact loading
 Acta Mech. Solida Sin., 30 (6) (2017), pp. 583-595
[CrossRef](#) [View Record in Scopus](#) [Google Scholar](#)
- [Luo et al., 2013](#) Fu Jia Luo, Li He, Pana Zhu, Hui Duana Wen, Ling Zhaoa Xiao, Frank Collins
Effect of very fine particles on workability and strength of concrete made with dune sand
 Construct. Build. Mater., 47 (2013), pp. 131-137
[Article](#)  [Download PDF](#) [View Record in Scopus](#) [Google Scholar](#)
- [Pliya et al., 2019](#) P. Pliya, D. Cree, H. Hajiloo, A.-L. Beaucour, M.F. Green, A. Noumowe
High-strength concrete containing recycled coarse aggregate subjected to elevated temperatures
 Fire Technol., 55 (5) (2019), pp. 1477-1494
[CrossRef](#) [View Record in Scopus](#) [Google Scholar](#)
- [Popovics, 1973](#) S. Popovics
A numerical approach to the complete stress-strain curve of concrete
 Cement Concr. Res., 5 (1973), pp. 583-599
[Article](#)  [Download PDF](#) [View Record in Scopus](#) [Google Scholar](#)
- [Qiu, 2019](#) Peng Qiu
Experimental research on fracture behavior of concrete after high temperature
 Frat. Ed. Integrità Strutt., 13 (50) (2019), pp. 300-309
[CrossRef](#) [View Record in Scopus](#) [Google Scholar](#)
- [Ren et al., 2015](#) Weibo Ren, Jinyu Xu, Erlei Bai
Strength and ultrasonic characteristics of alkali-activated fly ash-slag geopolymer concrete after exposure to elevated temperatures
 J. Mater. Civ. Eng., 28 (2) (2015), Article 04015124
[Google Scholar](#)
- [Shanxi Provincial Academy of Building Sciences, 2009](#) Shanxi Provincial Academy of Building Sciences
Standard for Test Methods of Basic Performance of Building Mortar (JCJ/T70-2009) [S]
 China Industrial Construction Press, Beijing (2009)
[Google Scholar](#)
- [Shen et al., 2019](#) Dejian Shen, Kaiqi Liu, Chuyuan Wen, Yongqiang Shen, Guoqing Jiang
Early-age cracking resistance of ground granulated blast furnace slag concrete
 Construct. Build. Mater., 222 (2019), pp. 278-287
[Article](#)  [Download PDF](#) [View Record in Scopus](#) [Google Scholar](#)
- [Singh et al., 2019](#) L.P. Singh, D. Ali, I. Tyagia, U. Sharmaa, R. Singhb, P. Hou

Durability studies of nano-engineered fly ash concrete

Construct. Build. Mater., 194 (2019), pp. 205-215

[Article](#)  [Download PDF](#) [View Record in Scopus](#) [Google Scholar](#)

[Sugiyama and Tsuji, 2008](#) Takafumi Sugiyama, Yukikazu Tsuji

Use of a migration technique to study alteration of compacted sand–bentonite mixture in contact with concrete

Phys. Chem. Earth, Parts A/B/C, 33 (2008), pp. S276-S284

[Article](#)  [Download PDF](#) [View Record in Scopus](#) [Google Scholar](#)

[Sun and Liu, 2018](#) Shuai Sun, Haifeng Liu

Experimental research on the splitting tensile strength of desert sand concrete after high temperature

Ind. Constr., 1 (2018), pp. 140-143

[View Record in Scopus](#) [Google Scholar](#)

[Sun and Miao, 2012](#) Wei Sun, Changwen Miao

Modern Concrete Theory and Technology [M]

Science Press (2012)

[Google Scholar](#)

[Tonelli et al., 2017](#) Monica Tonelli, F. Martini, L. Calucci, M. Geppi, S. Borsacchi, F. Ridi

Traditional Portland cement and MgO-based cement: a promising combination?

Phys. Chem. Earth, Parts A/B/C, 99 (2017), pp. 158-167

[Article](#)  [Download PDF](#) [View Record in Scopus](#) [Google Scholar](#)

[Tuinukuafe et al., 2019](#) Atolo Tuinukuafe, Kaubb Tyler, A. Charles, Jrd Weiss, Paul G. Allisone, Gregory B. Thompsonb, Armen Amirkhanian

Atom probe tomography of an alkali activated fly ash concrete

Cement Concr. Res., 121 (2019), pp. 37-41

[Article](#)  [Download PDF](#) [View Record in Scopus](#) [Google Scholar](#)

[Vijayaraghavan et al., 2017](#) J. Vijayaraghavan, A. Belin Jude, J. Thivya

Effect of copper slag, iron slag and recycled concrete aggregate on the mechanical properties of concrete

Resour. Pol., 53 (2017), pp. 219-225

[Article](#)  [Download PDF](#) [View Record in Scopus](#) [Google Scholar](#)

[Yan et al., 2019](#) Wenlong Yan, Gang Wu, Zhiqiang Dong

Optimization of the mix proportion for desert sand concrete based on a statistical model

Construct. Build. Mater., 226 (2019), pp. 469-482

[Article](#)  [Download PDF](#) [View Record in Scopus](#) [Google Scholar](#)

[Yang et al., 2014](#) Weiwu Yang, Yunlong Chen, Jurong Ma

Study on influence of desert sand replacement rate on compressive strength of high strength concrete

Sci. Technol. Eng., 14 (19) (2014), pp. 289-292

[View Record in Scopus](#) [Google Scholar](#)

[Yang et al., 2015](#) Weiwu Yang, Yunlong Chen, Haifeng Liu

Influence of desert sand replacement ratio on the compressive strength of high strength concrete from Mu Us desert

Sichuan Building Science, 41 (1) (2015), pp. 217-219

[CrossRef](#) [View Record in Scopus](#) [Google Scholar](#)

© 2020 Elsevier Ltd. All rights reserved.



[About ScienceDirect](#)

[Remote access](#)

[Shopping cart](#)

[Advertise](#)

[Contact and support](#)

[Terms and conditions](#)

[Privacy policy](#)

We use cookies to help provide and enhance our service and tailor content and ads. By continuing you agree to the **use of cookies**.

Copyright © 2021 Elsevier B.V. or its licensors or contributors. ScienceDirect® is a registered trademark of Elsevier B.V.

ScienceDirect® is a registered trademark of Elsevier B.V.



FEEDBACK